Design and investigation of the hydraulic performance of bionic hydrofoil based on the geometric features of sturgeons

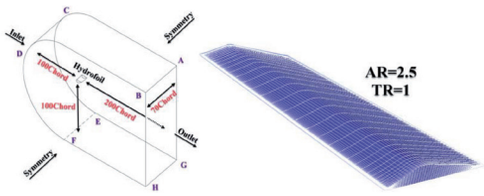

Diseño e investigación del comportamiento hidráulico del hidroala biónica a partir de las características geométricas de los esturiones

Hao Yan[1,2], Chao Yu[1,*], Liping Chai[1], Yunqing Li[1], Valentina Vnenkovskaia[3], and Hao Chen[4]

[1] School of mechanical engineering, Hefei University of Technology, Tunxi Road 193#, Hefei, 230009, Anhui, China
[2] Hefei huasheng pumps&tvalves co.,ltd, Jinhuai Road 06#, Hefei, 230009, Anhui, China
[3] Research and Production Centre "ANOD", Svobody street 63#, Nizhniy Novgorod,603003,Russia
[4] School of life science, Anhui Medical University, Meishan Road 81#, Hefei, 230032, Anhui, China
[*] Corresponding author: stevenyu_personal@163.com; Tel.: +86-0551-6290-1708

DOI: http://dx.doi.org/10.6036/9129 | Recibido: 25/02/2019 • Inicio Evaluación: 25/02/2019 • Aceptado: 25/03/2019

RESUMEN

- Los sustentadores diseñados por el Comité Consultivo Nacional de Aeronáutica (NACA) son actualmente adoptados en los hidroalas de propulsión hidráulica (bomba, turbina de agua). Sin embargo, la serie NACA está diseñada en base a la teoría de la aerodinámica, por lo que su rendimiento se ve afectado inevitablemente cuando se aplica directamente a la propulsión hidráulica. Por lo tanto, debemos investigar más a fondo, basándonos en organismos acuáticos, el mecanismo que afecta a las características hidrodinámicas del hidroala. En este estudio, se diseñó un hidroala basado en el esturión en medio acuático utilizando un escáner láser 3D y se integró el rendimiento hidrodinámico del hidroala mediante simulación numérica. Se adoptó un modelo SST k-w en los números 1E6, 3E6 y 5E6 de Reynolds bajo un ángulo de ataque de 0°-27° para el análisis de los coeficientes de elevación y resistencia, vórtices de punta y distribución de presión en la superficie superior del hidroala tipo esturión en comparación con los de los hidroala tipo NACA0012 y NACA0015. Los resultados muestran que los coeficientes de elevación del hidroala tipo esturión son mayores que los de los hidroala NACA0012 y NACA0015 en diferentes números de Reynolds. Los hidroala NACA0012 y NACA0015 generan y extienden vórtices de punta más fácilmente que el hidroala tipo esturión, pero éste genera una mayor fuerza de elevación antes de alcanzar el ángulo de pérdida del ataque, especialmente en la región de máximo espesor de la superficie superior. Las conclusiones obtenidas en el estudio tienen importantes implicaciones para el diseño de un perfil biónico adecuado para la propulsión hidráulica.
- **Palabras clave:** Hidroala biónica, Flujo de fluido, Vórtices de punta, Distribución de presión, Rendimiento hidrodinámico.

ABSTRACT

The airfoils designed by the National Advisory Committee for Aeronautics (NACA) are currently adopted in the blades of hydraulic machinery (pump, water turbine). However, the NACA series are designed on the basis of the aerodynamics theory, so their performance are inevitably affected when they are applied directly to hydraulic machinery. Thus, the mechanism affecting the hydrodynamic characteristics of a hydrofoil based on aquatic organisms must be further investigated. In this study, a sturgeon hydrofoil based on the water environment was designed by using a 3D laser scanner, and the hydrodynamic performance of the hydrofoil was integrated by numerical simulation. A k–ω SST model was adopted at Reynolds numbers 1E6, 3E6, and 5E6 under 0°–27° angle of attack for the analysis of the lift and drag coefficients, tip vortices, and pressure distribution on the upper surface of the sturgeon hydrofoil as compared with those of the NACA0012 and NACA0015 hydrofoils. Results show that the lift coefficients of the sturgeon hydrofoil are greater than those of the NACA0012 and NACA0015 hydrofoils at different Reynolds numbers. The NACA0012 and NACA0015 hydrofoils generate and spread tip vortices easier than the sturgeon hydrofoil, but the sturgeon hydrofoil generates a larger lift force before reaching the stall angle of attack, especially in the maximum-thickness region on the upper surface. Conclusions obtained in the study have important implications for designing a bionic airfoil suitable for hydraulic machinery.

Keywords: Bionics hydrofoil, Fluid flow, Tip vortices, Pressure distribution, Hydrodynamic performance.

1. INTRODUCTION

Energy has attracted considerable attention from researchers worldwide. Meanwhile, characterized by the large quantity and wide distribution[1-2], general machinery (pump, turbine, and compressor) is the basic equipment for energy transmission, and its efficient operation is crucial to energy conservation[3]. The blade section of general machinery is primarily composed of profiles in the shape of hydrofoils, which influence the hydraulic performance of pumps, water turbines, and autonomous systems, including autonomous underwater vehicles and underwater gliders. Hydrofoils prevent the generation of noises, tip vortices, and even cavitation inception to some extent and thus minimize energy loss[4].

For millions of years in evolution, aquatic animals have necessarily developed sophisticated ways of moving rapidly while reducing energy consumption[5]. Bionic hydrofoils efficiently produce high thrust with minimal noise[6] and therefore has broad applications in underwater vehicles[7]. In fact, the sturgeon is an ancient actinopterygian fish that appeared in the Upper Cretaceous Period and has adapted to life in an underwater environment[8]. The body structures and appearances of sturgeons differ from those of other aquatic vertebrates. A toothed whale (e.g., dolphins, beluga whales, and orcas) has a hydrodynamic body and has a large melon-shaped structure behind its rostrum. By contrast, a

sturgeon has a cobbly body and the melon-shaped structure is absent. Hence, the heads of sturgeons may have less drag force than those of common cetaceans. Moreover, sturgeons can leap out of water at high altitudes to show courtship, catch airborne prey, or shed parasites[9]. This ability shows that the curve shape of the sturgeon can reduce drag to some degree.

This study aims to identify the curve shape of the sturgeon and investigate the hydrodynamic performance of the sturgeon hydrofoil. Inspired by a previous work, we integrated scanned, measured, and numerically simulated data to evaluate the hydrodynamic performance of sturgeon hydrofoils. The lift and drag behaviors of a sturgeon were scanned and evaluated. Then, sturgeon hydrofoils were compared with NACA0012 and NACA0015 hydrofoils, which have been demonstrated to exhibit excellent hydrodynamic performance by Malti K et al.[10]. The hydrodynamic performance of the hydrofoils was analyzed.

2. STATE OF THE ART

Bionic hydrofoils, as well as the flippers of aquatic animals, have been extensively investigated. For example, Weber et al.[11] scanned the cetacean flippers and tested their 3D geometry via water tunnels; they discovered that the lift and drag curves of the cetacean flippers resemble those of modern hydrofoil control surfaces found in engineering facilities. Thus, flippers can be used as bionic hydrofoils in the field of hydraulic machinery. They only analyzed the lift and drag characteristics of the cetacean flippers but did not consider the influence of tip vortices and pressure distribution on the hydraulic performance of the cetacean flippers. Fish et al.[12-14] found that the lateral section of a representative flipper resembles that of a modern engineered airfoil or hydrofoil. Flippers stabilize the body during swimming and are conducive to all types of underwater movements, such as braking, diving, lateral turning, rolling, paddling, and surfacing. The hydraulic performance and the lift and drag characteristics of flippers in whales have been analyzed, but their potential application in the field of hydraulic machinery remains unexplored. Cooper et al.[15] established the cetacean flipper model and tested its hydrodynamic performance under different angles of attack and swimming speeds; they found that flippers are crucial to improving flexibility. In addition to the flippers of whales, the forelimbs of other aquatic animals have been extensively studied. In particular, relational research has been conducted to establish a mathematical model for turtle propulsion on the basis of the characteristics of the hydrofoil motion of turtles. They established a motion model and validated the feasibility of bionic propulsive principle and the reliability of the biomechanism[16-18]. However, they only analyzed the turtle's motion trajectory from the perspective of kinematics, excluding the hydraulic performance of the turtle's forelimbs, and did not consider the combination with the application in the field of hydraulic machinery. In addition, many numerical and experimental methods were applied to investigate the hydraulic performance of hydrofoils[19]. Nowruzi H et al.[20] analyzed the lift and drag characteristics of 2D and 3D submerged hydrofoils and performance prediction with optimal artifical neural networks(ANNs) by using OpenFOAM; they found that a larger value of aspect ratio(AR) and a lower taper ratio(TR) lead to a greater lift to drag ratio(LDR) for 3D hydrofoils. However, they did not analyze the tip vortices and pressure distribution. The formation mechanism of tip vortices and the pressure distribution of hydrofoils could provide references for noise and cavitation reduction. Ghassemi et al.[21-22] and Xie et al.[23] studied the hydrofoil performance of 3D NACA4412 by numerical simulation. They analyzed the lift and drag characteristics and pressure distribution, excluding the tip vortices. Djavareshkian et al.[24-25] analyzed and compared the hydrodynamic performance of smart hydrofoil and a conventional hydrofoil. They found that smart hydrofoils generate a higher lift to drag ratio. However, they did not realize that the tip vortices and pressure distribution affect the hydraulic performance of hydrofoils.

As such, the hydraulic performance of flippers and bionic hydrofoils with different structural forms were researched to some extent. Sturgeons have cobbly bodies and no melon-shaped structures in their heads. Hence, their heads may have less drag force than those of common cetaceans. Moreover, applying the curve shape of sturgeons to hydraulic machinery, particularly in axial-flow pumps, may improve hydraulic performance. Currently, bionic hydrofoils are rarely used in hydraulic machinery, and, when used,

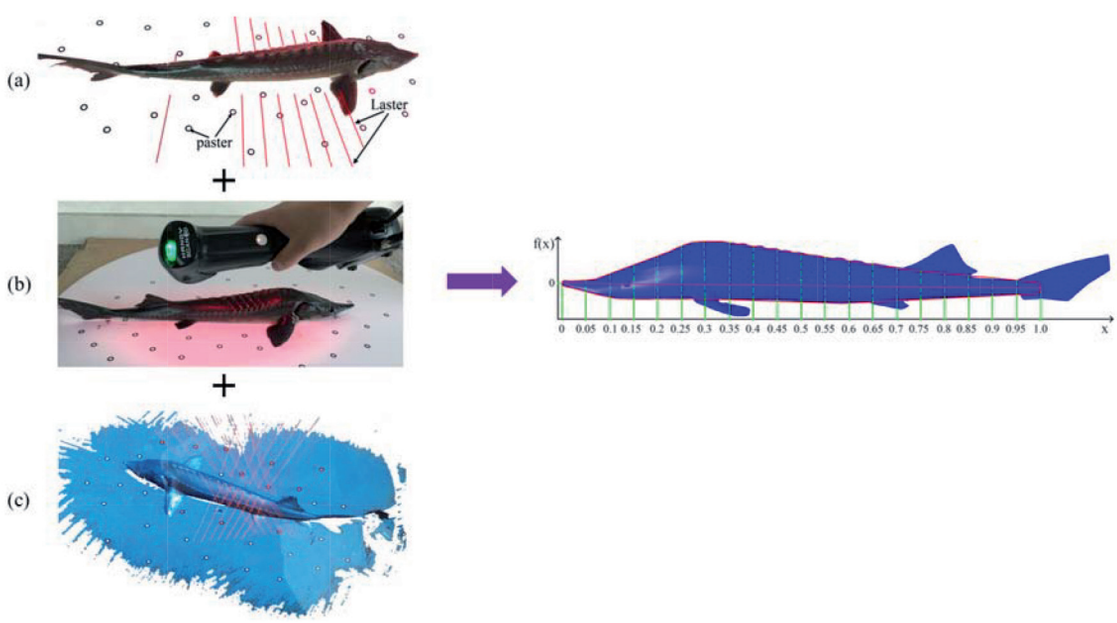

Fig. 1. (a) scanning plasters pasted on the table around the body of the sturgeon; (b) actual sturgeon scanned with 3D laser scanner; (c) scanned point cloud; (d) design of a bionic hydrofoil

show poor results. In the present study, a sturgeon hydrofoil based on the water environment is designed using a 3D laser scanner and integrate its hydrodynamic performance by numerical simulation. Moreover, the lift and drag coefficients, tip vortices, and pressure distribution on the upper surface of the sturgeon hydrofoil are analyzed at Reynolds numbers 1E6, 3E6, and 5E6 under 0° to 27° angle of attack and then compared with those of the NACA0012 and NACA0015 hydrofoils to show the advantages of the bionic hydrofoil and obtain the key factors that impact the hydraulic performance of the three hydrofoils. The results of this study serve as a reference for the design of hydraulic mechanical hydrofoils.

The remainder of this manuscript is organized as follows. Section 3 describes the design of bionic hydrofoil and the numerical method and grid independence test. We also compare the simulation data of NACA0012 and NACA0015 with the experimental data to verify the reliability of the simulation in this section. In section 4, *k*–ω *SST* model is adopted at Reynolds numbers 1E6, 3E6, and 5E6 under 0° to 27° angle of attack to analyze the lift and drag coefficients, tip vortices, and pressure distribution on the upper surface of the sturgeon hydrofoil in comparison with those of the NACA0012 and NACA0015 hydrofoils. Finally, conclusions are presented in section 5.

3. METHODOLOGY

3.1 BIONIC HYDROFOIL DESIGN

Three different body sizes of sturgeon were selected for scanning. These sturgeons are obtained from a sturgeon-breeding base in Anhui Province, China. The three sturgeons are freely stretched, placed on a round table, a number of scanning plasters are pasted on the table around the body of the sturgeon to collect structural features of the sturgeon shown in Figure 1(a) and three sturgeons are scanned using a non-contact 3D laser scanner shown in Figure 1(b). The scanning accuracy of the 3D laser scanner reaches 0.03 mm. To ensure scanning authenticity of each sturgeon's physical size, we scan each of them thrice. Then, the scanned point cloud is imported into the reverse engineering software Geomagic Design X in Figure 1(c), and the actual 3D sturgeon model is obtained. The tip of the rostrum denotes the origin of the coordinates, and the line from the tip of the rostrum to the tail denotes the X-axis. Figure 2(d) shows that the sturgeon along the X-axis is divided 20 times, and 40 control point coordinates are obtained; the obtained control points from each scan are dimensionless.

The scanned upper and lower surfaces coordinates of the sturgeon hydrofoil are defined as $(x_s, f_u(x_s))$ and $(x_s, f_l(x_s))$, respectively. $f_u(x_s)$ and $f_l(x_s)$ represent the ordinates of the upper and lower surfaces of the sturgeon model, where $(x_d, f_u(x_d))$ and $(x_d, f_l(x_d))$ are the dimensionless upper and lower surfaces coordinates, respectively. The relationship between the variables is defined as follows:

$$f(x_d) = \frac{f(x_s)}{C} \tag{1}$$

where C is the chord length of the sturgeon model.

Finally, the least squares method is used to fit the dimensionless control points. The details are as follows:

$$f(x) = b_0 + b_1 x \tag{2}$$

$$b_1 = \frac{\sum_{i=1}^{n} x_i f(x_i) - n\bar{x}_i \bar{f}(x_i)}{\sum_{i=1}^{n} x_i^2 - n(\bar{x})^2}, (n = 9) \tag{3}$$

$$b_0 = \bar{f}(x) - b_1 \bar{x} \tag{4}$$

x_d	0	0.05	0.1	0.15	0.2	0.25	0.3	0.35	0.4	0.45	0.5
$\lvert f_u(x_d)\rvert$	0	0.0155	0.0339	0.0540	0.0759	0.0972	0.1028	0.1012	0.0942	0.0865	0.0788
$\lvert f_l(x_d)\rvert$	0	0.0077	0.0096	0.0098	0.0091	0.0101	0.0101	0.0101	0.0100	0.0098	0.0095
x_d	0.55	0.6	0.65	0.7	0.75	0.8	0.85	0.9	0.95	1.0	
$\lvert f_u(x_d)\rvert$	0.0710	0.0633	0.0555	0.0478	0.0401	0.0323	0.0246	0.0168	0.0091	0	
$\lvert f_l(x_d)\rvert$	0.0092	0.0088	0.0084	0.0078	0.0073	0.0066	0.0058	0.0051	0.0042	0	

Tab I. Fitted control point coordinates of the sturgeon hydrofoil

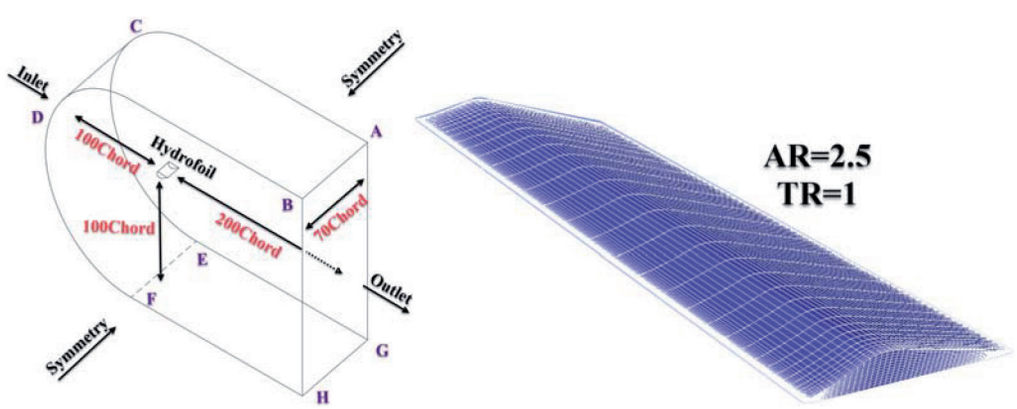

Fig. 2. (a) Boundary conditions of the computational domain and (b) mesh of sturgeon hydrofoil

Boundary Type	Location	Variable	Value
Inlet	ABCD, CDEF, and EFGH	Velocity	9.18m/s, 27.5m/s, and 45.9m/s
Outlet	ABHG	Outflow	-
Wall	Hydrofoil	No-slip	-
Symmetry	BDFH, ACEG	-	-

Tab II. List of boundary conditions

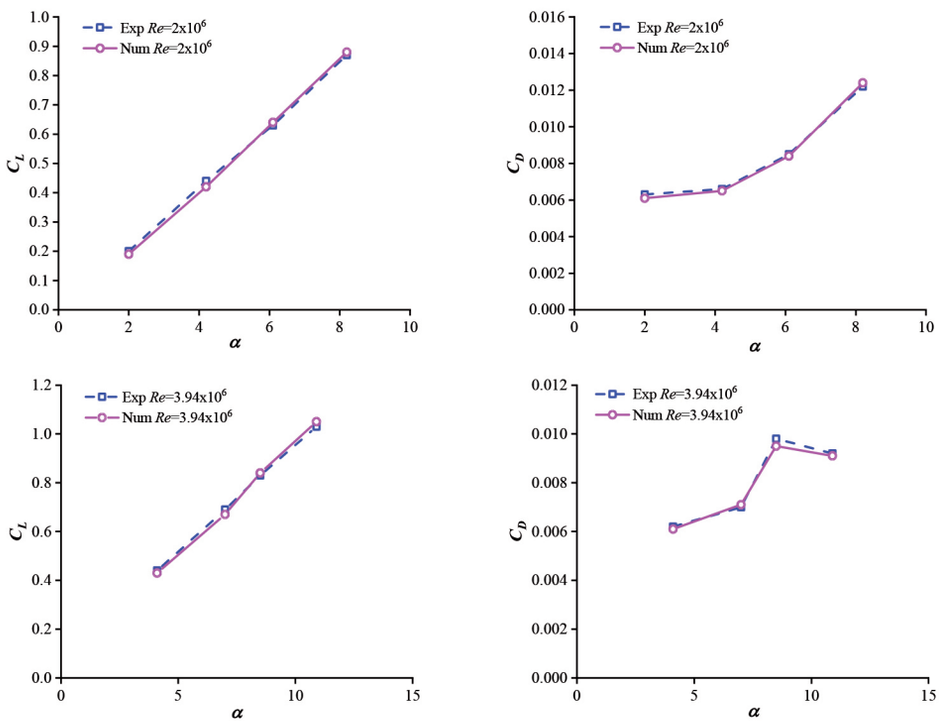

Fig. 4. Lift and drag coefficients of NACA0012 hydrofoil under different angles of attack at Reynolds numbers 2E6 and 3.94E6

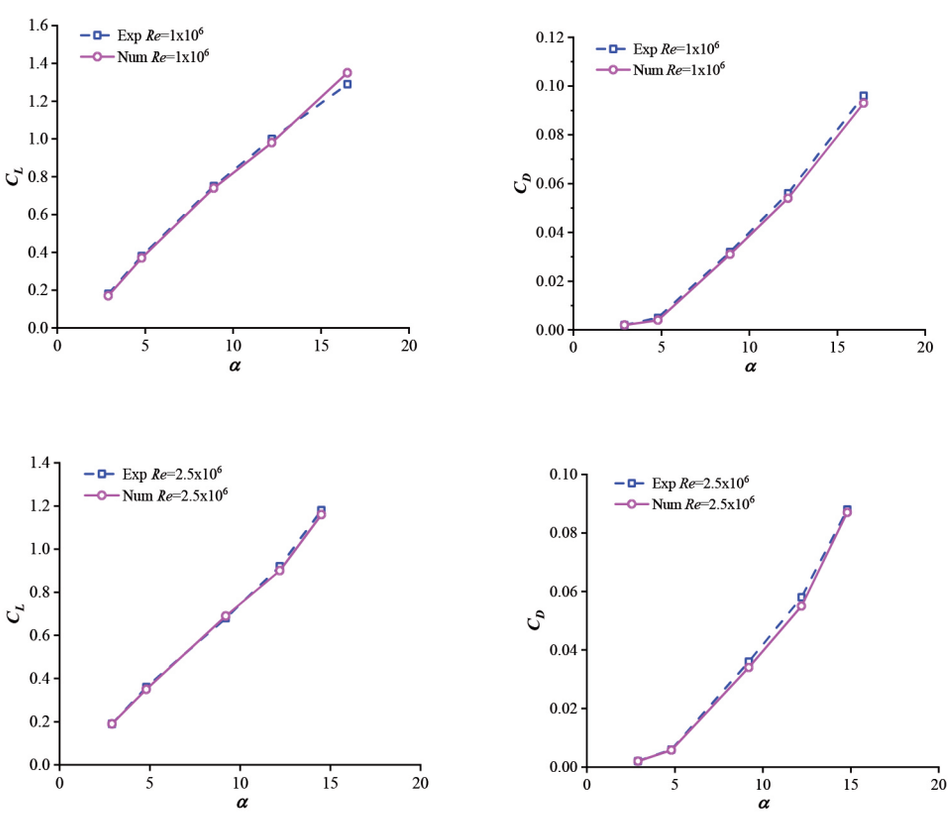

Fig. 5. Lift and drag coefficients of NACA0015 hydrofoil under different angles of attack at Reynolds numbers 1E6 and 2.5E6

$$\overline{x}=\frac{1}{n}\sum_{i=1}^{n}x_i,\ \overline{f}(x)=\frac{1}{n}\sum_{i=1}^{n}f(x_i) \quad (5)$$

where b_0 and b_1 are defined as constants of Equation (2), and n = 9 represents the nine sets of data. Coordinates of the fitted control points are obtained from Equation (2). Table I lists the fitted control point coordinates of the sturgeon hydrofoil. Some organs are not included in the bionic hydrofoil designed in consideration of the sturgeon's special biological characteristics. For example, sturgeons have four barbels, which are used for navigation and preying[26]. Therefore, the sturgeon hydrofoil has a modified curve that consists of control points on the middle plane of the sturgeon, except the tail, fins, and barbels, as shown in Figure 1.

3.2 NUMERICAL METHOD AND GRID INDEPENDENCE TEST

In this study, a 3D hydrofoil is subjected to flow with velocity U, and a particular angle of attack is defined as α. d is the pipe diameter, and the Reynolds number is defined as follows:

$$R_e=\frac{\rho U d}{\mu} \quad (6)$$

where ρ and u are the density of the fluid and dynamic viscosity coefficient, respectively.

Lift (C_L) and drag (C_D) force coefficients are defined as follows:

$$C_L=\frac{2L}{\rho U^2 S} \quad (7)$$

$$C_D=\frac{2D}{\rho U^2 S} \quad (8)$$

where ρ and S are the density of the fluid and relevant hydrofoil surface area, respectively.

At present, turbulence models in marine engineering have been considerably researched. Menter blended the *k*–ε turbulence model[27] in free stream and Wilcox's *k*–**ε** model near the wall and found that the *k*-*omega* model had good performance and natural treatment for near-wall boundary layers, while overcoming

its drawback of strong sensitivity to inlet turbulence conditions[28-29]. In this current study, the consequences from the *k-omega SST* model are provided for completeness, given the series of applications that have adopted it. Thus, the *k-omega SST* turbulence model is used to calculate the following bionic hydrofoils.

The results are computed using ANSYS fluent 16.0 code, and referenced data are used to study the bionic hydrofoils. Figure 2(a) shows the computational domain. The surface of the inlet indicates the velocity inlet, and the boundary of the outlet indicates the outflow condition. Meanwhile, the hydrofoil is defined as a wall under no-slip boundary conditions. Table II lists the boundary conditions of the simulation. For preventing the impact of the boundary on the solution, the computational domain must be considerably larger than that of the hydrofoil. Figure 2(b) shows that the simulation model of sturgeon hydrofoil adopts structured grid. AR and TR are set as 2.5 and 1.0, respectively.

Grid independence test for the NACA0015 hydrofoil is conducted to assess the effects of grid sizes on the results. Four kinds of mesh are generated using structured grids with 2,425,362; 1,718,814; 1,407,934; and 821,381 nodes. Figure 3(see section: supplementary material) shows the lift coefficients under different angles of attack. AR and TR are set as 3.28 and 1.0, respectively. The Reynolds number is 1E6. The root mean square error(RMSE) between nodes 1,718,814 and nodes 2,425,362 is 0.0126, it is indicated that the differences between nodes 1,718,814 and nodes 2,425,362 can be neglected. It should also be noted that any further grid refinement leads to smaller RMSE, while will require more computational resources. This is not however the focus of this study and is the subject of future work. Therefore, a domain with 1,718,814 nodes is selected to increase the calculation accuracy and decrease the computing time. Moreover, the numbers of nodes of the NACA0012 and the sturgeon hydrofoils are similar to that of the NACA0015 hydrofoil.

3.3 NUMERICAL VALIDATIONS

Numerical validations have been conducted by Şahin et al.[30] and Zhang et al.[31], and their results are compared with experimental ones. Simulation, as explained in the previous section, is adopted. Numerical consequences on the lift and drag coefficients of NACA0012 and NACA0015 hydrofoils under different angles of attack and Reynolds number are compared with the experimental ones shown in Figures 5 and 6. AR = 1.521 and AR = 3.28 are selected in the simulation of the NACA0012 and NACA0015 hydrofoils, respectively, wherein both are TR = 1. The illustrated plots indicate consistent results between experimental and numerical simulations. We also calculate the root mean square error between the simulation results and the experimental results. The maximum root mean square error between numerical results and experimental data is very small. Therefore, the numerical method is reliable.

The same numerical method and boundary condition are conducted on the sturgeon, NACA0012, and NACA0015 hydrofoils. Furthermore, numerical analysis is conducted on the lift and drag coefficients of these hydrofoils under different Reynolds numbers. Figure 6 shows the results. Moreover, the velocity field on the surface of the hydrofoils and the pressure distribution in the middle cross sections are analyzed by comparing the sturgeon hydrofoil with the NACA0012 and NACA0015 hydrofoils, as shown in Figures 9 and 10.

4. RESULT ANALYSIS

4.1 LIFT AND DRAG COEFFICIENTS

Figure 6 shows the simulation of the lift and drag coefficients for the three abovementioned types of hydrofoils under different angles of attack. Aspect and thickness ratios are set as 2.5 and 1.0, respectively. In addition, Reynolds numbers 1E6, 3E6, and 5E6 are adopted. Figure 7 shows the lift and drag coefficients of the three types of hydrofoils under different angles of attack. The sturgeon hydrofoil obtains the greatest and lowest lift and drag coefficients, respecti-

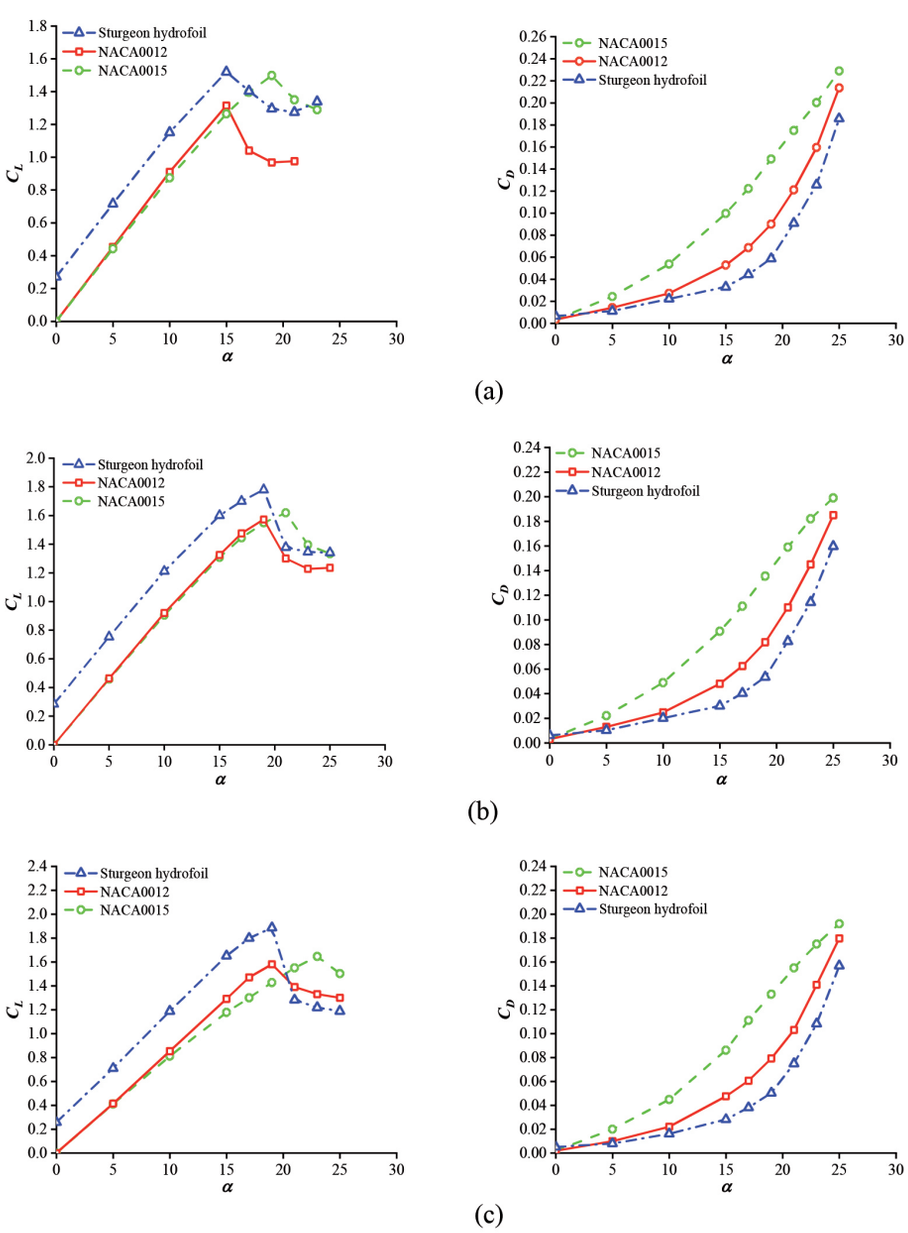

Fig. 6. Lift and drag coefficients of the three types of hydrofoils under different angles of attack at Reynolds numbers (a) 1E6; (b) 3E6; and (c) 5E6

vely. Stall angles of attack of the sturgeon hydrofoil are 15°, 17°, and 19° under Reynolds numbers 1E6, 3E6, and 5E6, respectively, similar to those of the NACA0012 hydrofoil but smaller than those of the NACA0015 hydrofoil. Furthermore, the sturgeon hydrofoil has a greater hydrodynamic performance than that of the NACA0012 hydrofoil but runs into stall earlier than that of the NACA0015 hydrofoil. The three hydrofoils are compared under different Reynolds numbers. Lift coefficients are increased due to the increase in Reynolds number, thereby indicating that the stall angle of attack may also increase by increasing the Reynolds number. As the Reynolds number increases, the liquid begins to flow less smoothly over the upper surface of the hydrofoil, thereby delaying the boundary layer separation of the hydrofoil surface and increasing the stall angle of attack.

4.2 VELOCITY FIELD AND PRESSURE DISTRIBUTION

Velocity field and pressure distribution are also crucial in analyzing the hydrodynamic performance of hydrofoils. To obtain a good understanding of the results, the parameters are defined as follows:

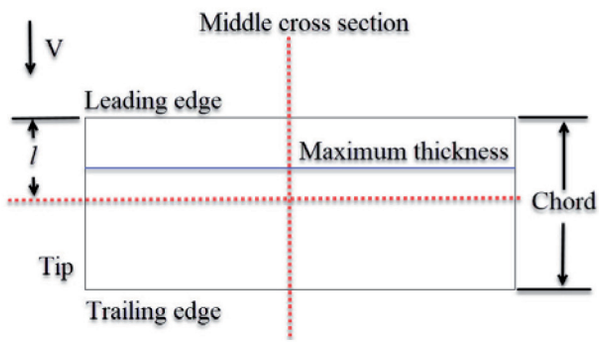

Fig. 7. Profile of the hydrofoil structure (vertical view)

Figure 7 shows that l is the distance between the leading edge and cross sections, and D is defined as follows:

$$D = \frac{l}{C} \tag{9}$$

where C is the length of the chord.

This subsection shows the results of the three types of hydrofoils at 10° angle of attack and Reynolds number 5.0E6. Velocity vectors are shown in different cross sections of the hydrofoil, depending on the distance from the leading edge. Figure 8 shows the velocity vector of the sturgeon hydrofoil, and those of NACA0012 and NACA0015 hydrofoils are shown in the middle and right columns, respectively. Researchers have obtained the vortices generated around the tip area and conclude that the tip vortices must rotate and move to the upper surface of the hydrofoil. This area may lead to cavitation inception[32].

Figure 8 shows that the three types of hydrofoils have similar results. However, varied details exist among the hydrofoils. Figure 8(e) shows that the last section in the left column (sturgeon hydrofoil), which is the nearest cross section from the trailing edge, and velocity vectors tend to rotate shifts more to the left region of the hydrofoil compared with those of the NACA0012 and NACA0015 hydrofoils. Tip vortices of the sturgeon hydrofoil are smaller than those of NACA0012 and NACA0015 hydrofoils in all of the cross sections; therefore, the NACA0012 and NACA0015 hydrofoils may generate and spread tip vortices easier than that of the sturgeon hydrofoil, leading to cavitation. However, good hydrodynamic performance of the middle region on the upper surface remains

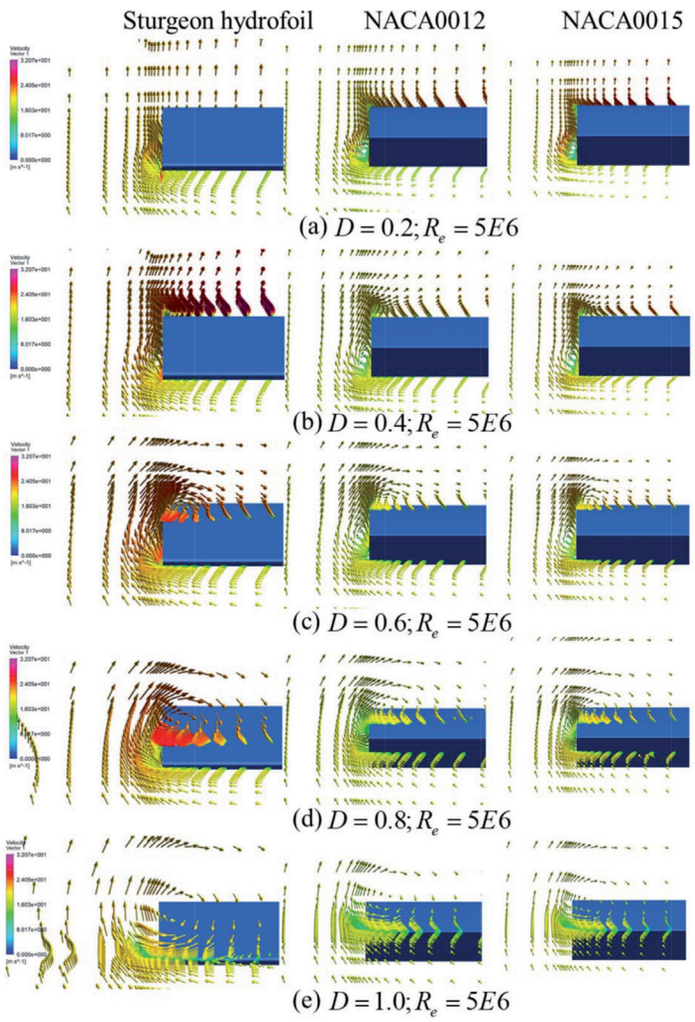

Fig. 8. Velocity field around the sturgeon (left column), NACA0012 (middle column), and NACA0015 (right column) hydrofoil cross sections at Reynolds number 5E6: (a) D = 0.2; (b) D = 0.4; (c) D = 0.6; (d) D = 0.8; (e) D = 1.0

uncertain. Therefore, the following section analyzes the pressure distribution in the middle cross section of the hydrofoil.

Figure 9 shows the pressure distribution in the intersection line of the middle cross section and hydrofoil for the three types of hydrofoils at Reynolds number 3.0E6 and angles of attack selected from 5° to 20°. D is defined in Figure 7, and maximum thickness represents the region of the sturgeon hydrofoil with maximum thickness of $D = 0.28$. Notably, variations of the lift and drag forces depend on the pressure distribution on the surface of the hydrofoil. Pressure distribution is also crucial in obtaining the cavitation or other adverse effects of the hydrofoil. Hence, these plots must be analyzed accurately. Figure 9 shows that the NACA0012 and NACA0015 hydrofoils have similar plots. As the angle of attack increases, the pressure difference on the upper and lower surfaces also increases, thereby generating an enhanced lift force[33]. Therefore, the sturgeon hydrofoil generates a larger lift force than those of the NACA0012 and NACA0015 hydrofoils at the 5°, 10°, and 15° angles of attack, especially in the maximum-thickness region, thereby potentially leading to the generation of vortices. However, the 20° angle of attack is greater than the stall angle of attack of the sturgeon hydrofoil, and the pressure difference on the upper and lower surfaces decreases suddenly. Hence, the sturgeon hydrofoil has a better hydrodynamic performance than those of the NACA0012 and NACA0015 hydrofoils before reaching the stall angle of attack.

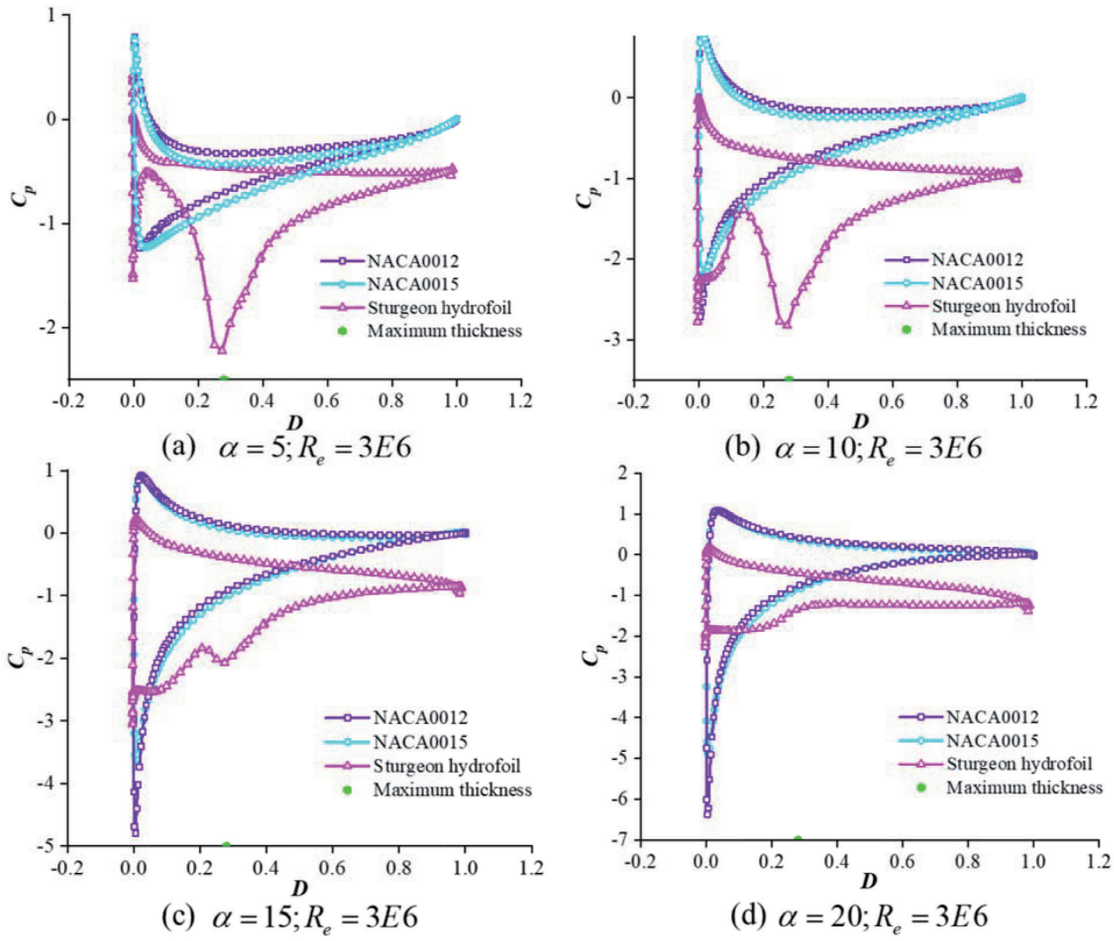

Fig. 9. Pressure distribution in the intersection line of the middle cross section and hydrofoil at Reynolds number 3E6: (a) α = 5°; (b) α = 10°; (c) α = 15°; (d) α = 20°

5. CONCLUSION

Although the bionic hydrofoils of aquatic vertebrates such as whales and dolphins, have been designed and applied, the hydrodynamic performance of the sturgeon hydrofoil is seldom documented. To discover the superiority of the bionic hydrofoil's hydraulic performance and be better applied in hydraulic machinery, in this study, we use the numerical simulation to investigate the lift and drag coefficients, tip vortices, and pressure distribution of the sturgeon hydrofoil. The following conclusions can be drawn:

(1) The lift and drag coefficients of the sturgeon hydrofoil are compared with those of the NACA0012 and NACA0015 hydrofoils. When the Reynolds number is increased with the lift coefficients and stall angles of attack, the lift coefficients of the sturgeon hydrofoil are consistently greater than those of the NACA0012 and NACA0015 hydrofoils. The stall angles of attack of the sturgeon hydrofoil are 15°, 17°, and 19° at Reynolds numbers 1E6, 3E6, and 5E6, respectively, similar to that of the NACA0012 hydrofoil but smaller than that of the NACA0015 hydrofoil.

(2) The tip vortices are analyzed and obtained a negative effect, leading to generating noises or even cavitation inception. Velocity vectors tend to rotate shifts more to the left region of the hydrofoil in the nearest cross section from the trailing edge, as compared with those of the NACA0012 and NACA0015 hydrofoils. Tip vortices of the sturgeon hydrofoil are smaller than those of NACA 0012 and NACA0015 hydrofoils in the rest of the cross sections, thereby indicating that NACA0012 and NACA0015 hydrofoils generate and spread tip vortices easier than the sturgeon hydrofoil at the tip.

(3) The sturgeon hydrofoil generates a larger lift force than the NACA0012 and NACA0015 hydrofoils at the 5°, 10°, and 15° angles of attack. The pressure distribution in the intersection line of the middle cross section and hydrofoil indicates that the sturgeon hydrofoil generates a larger lift force than the NACA0012 and NACA0015 hydrofoils before reaching the stall angle of attack, especially in the region of maximum thickness on the upper surface.

In this study, the sturgeon hydrofoil demonstrates a relatively better hydrodynamic performance than those of the NACA0012 and NACA0015 hydrofoils, as indicated by the simulation results. The results can provide important references to the efficiency optimization of transmission equipment in fluid machinery. However, given the lack of visualized experimental data of the sturgeon hydrofoil under different Reynolds number, future experimental studies can integrate the particle image velocimetry for their contrastive analysis; this integration is conducive to the systematic analysis on the advantages of the bionic hydrofoil.

REFERENCES

[1] Fan Y, Mu A, Ma T. "Study on the Application of Energy Storage System in Offshore Wind Turbine with Hydraulic Transmission". Energy Conversion and Management. February 2016. Vol. 110-15. p.338-346. DOI: https://doi.org/10.1016/j.enconman.2015.12.033

[2] Giallanza A, Porretto M, Cannizzaro L, et al. "Analysis of the Maximization of Wind Turbine Energy Yield Using a Continuously Variable Transmission System". Renewable Energy. March 2017. Vol. 102. p.481-486. DOI: https://doi.org/10.1016/j.renene.2016.10.067

[3] Ruan X, Ma Q, Lv X, et al. "Design and Experimental Study on the Automatic Speed Control System of a Pneumatic Submersible Pump". Journal of

Engineering Science & Technology Review. January 2017. Vol. 10-4. p.25-30. DOI: https://doi.org/10.25103/jestr.104.04
[4] Arndt R E A, Arakeri V H, Higuchi H. "Some observations of tip-vortex cavitation". Journal of fluid mechanics. August 1991. Vol. 229. p.269-289. DOI: https://doi.org/10.1017/S0022112091003026
[5] Cooper L N, Sedano N, Johansson S, et al. "Hydrodynamic Performance of the Minke Whale (Balaenoptera Acutorostrata) Flipper". Journal of Experimental Biology. April 2008. Vol. 211-12. p.1859-1867. DOI: https://doi.org/10.1242/jeb.014134
[5] Font D, Tresanchez M, Siegentahler C, et al. "Design and implementation of a biomimetic turtle hydrofoil for an autonomous underwater vehicle". Sensors. November 2011. Vol. 11-12. p.11168-11187. DOI: https://doi.org/10.3390/s111211168
[7] Xu J, Yan N, Zhang M. "Analysis of Bionic Hydrofoil Propulsive Performance". In proceedings of the 2011 IEEE International Conference on Mechatronics and Automation. August 2011. p.1418-1422. DOI: https://doi.org/10.1109/ICMA.2011.5985784
[8] Sulak K J, Berg J J, Randall M. "Feeding Habitats of the Gulf Sturgeon, Acipenser Oxyrinchus Desotoi, in the Suwannee and Yellow Rivers, Florida, as Identified by Multiple Stable Isotope Analyses". Environmental Biology of Fishes. October 2012. Vol. 95-2. p.237-258. DOI: https://doi.org/10.1007/s10641-012-9986-4
[9] Sulak K J, Edwards R E, Hill G W. "Why Do Sturgeons Jump? Insights from Acoustic Investigations of the Gulf Sturgeon in the Suwannee River, Florida, USA". Journal of Applied Ichthyology. December 2002. Vol. 18. p.617-620. DOI: https://doi.org/10.1046/j.1439-0426.2002.00401.x
[10] Malti K, Hebow H, Imine B. "Numerical study of flow around NACA0015 in ground effect". In proceedings of the 10th Anniversary International Conference on Experimental Fluid Mechanics. November 2015. Vol. 114. p.02069. DOI: https://doi.org/10.1051/epjconf/201611402069.
[11] Weber P W, Howle L E, Murray M M, et al. "Lift and Drag Performance of Odontocete Cetacean Flippers". Journal of Experimental Biology. July 2009. Vol. 212-14. p.2149-2158. DOI: https://doi.org/10.1242/jeb.029868
[12] Fish, Frank E. "Balancing Requirements for Stability and Maneuverability in Cetaceans". Integrative and Comparative Biology. February 2002. Vol. 42-1. p.85-93. DOI: https://doi.org/10.1093/icb/42.1.85
[13] Fish, Frank E, Lauder G V. "Passive and Active Flow Control by Swimming Fishes and Mammals". Annual Review of Fluid Mechanics. January 2006. Vol. 38. p.193-224. DOI: https://doi.org/10.1146/annurev.fluid.38.050304.092201
[14] Fish, Frank E. "Biomechanics and Energetics in Aquatic and Semiaquatic Mammals: Platypus to Whale". Physiological and Biochemical Zoology. November 2000. Vol. 73-6. p.683-698. DOI: https://doi.org/10.1086/318108
[15] Cooper L N, Dawson S D, Reidenberg J S, et al. "Neuromuscular Anatomy and Evolution of the Cetacean Forelimb". The Anatomical Record: Advances in Integrative Anatomy and Evolutionary Biology. September 2007. Vol. 290-9. p.1121-1137. DOI: https://doi.org/10.1002/ar.20571
[16] Xu J A, Sun L N, Zhao W D, et al. "Bionic Research of Turtle Hydrofoil Propulsion". Key Engineering Materials. September 2010. Vol. 450. p.95-98. DOI: https://doi.org/10.4028/www.scientific.net/KEM.450.95
[17] Zhang M, Liu X, Chu D, et al. "The Principle of Turtle Motion and Bio-Mechanism of Its Four Limbs Research". In proceedings of 2008 IEEE Pacific-Asia Workshop on Computational Intelligence and Industrial Application. December 2008. p.1534-1539. DOI: https://doi.org/10.1109/paciia.2008.312
[18] Chu D, Liu X, Zhang M. "Research on Motion Principle and Bionics". In proceedings of the IEEE International Conference on Automation and Logistics. August 2007. p.2373-2378. DOI: https://doi.org/10.1109/lcal.2007.4338974
[19] Wei Q, Chen H, Zhang R. "Numerical Research on the Performances of Slot Hydrofoil". Journal of hydrodynamics. February 2015. Vol. 27-1. p.105-111. DOI: https://doi.org/10.1016/S1001-6058(15)60462-0
[20] Nowruzi H, Ghassemi H, Ghiasi M. "Performance Predicting of 2d and 3d Submerged Hydrofoils Using Cfd and Anns". Journal of Marine Science and Technology. December 2017. Vol. 22-4. p.710-733. DOI: https://doi.org/10.1007/s00773-017-0443-0
[21] Ghassemi H, Iranmanesh M, Ardeshir A. "Simulation of Free Surface Wave Pattern Due to the Moving Bodies". Iranian Journal of Science and Technology. April 2010. Vol. 34-B2. p.117-134. DOI: https://doi.org/10.22099/IJSTM.2010.906
[22] Ghassemi H, Ghamari I, Ashrafi A. "Numerical prediction of wave patterns due to motion of 3D bodies by kelvin-havelock sources". Polish Maritime Research. December 2016. Vol. 23-4. p.46-58. DOI: https://doi.org/10.1515/pomr-2016-0069
[23] Xie N, Vassalos D. "Performance Analysis of 3d Hydrofoil under Free Surface". Ocean Engineering. June 2007. Vol. 34-8. p.1257-1264. DOI: https://doi.org/10.1016/j.oceaneng.2006.05.008
[24] Djavareshkian M H, Esmaeili A. "Neuro-Fuzzy Based Approach for Estimation of Hydrofoil Performance". Ocean Engineering. February 2013. Vol. 59-1. p.1-8. DOI: https://doi.org/10.1016/j.oceaneng.2012.10.015
[25] Djavareshkian M H, Esmaeili A, Parsania A. "Numerical Simulation of Smart Hydrofoil in Marine System". Ocean Engineering. November 2013. Vol. 73-16. p.16-24. DOI: https://doi.org/10.1016/j.oceaneng.2013.07.015
[26] Lauder G V. "Function of the caudal fin during locomotion in fishes: kinematics, flow visualization, and evolutionary patterns". American Zoologist. August 2015. Vol. 40-1. p.101-122. DOI: https://doi.org/10.1093/icb/40.1.101
[27] Menter F R. "Two-Equation Eddy-Viscosity Turbulence Models for Engineering Applications". AIAA Journal. August 1994. Vol. 32-8. p.1598-1605. DOI: https://doi.org/10.2514/3.12149
[28] Wilcox D C. "Reassessment of the scale-determining equation for advanced turbulence models". AIAA journal. November 1988. Vol. 26-11. p.1299-1310. DOI: https://doi.org/10.2514/3.10041
[29] Muiruri P I, Motsamai O S. "Three Dimensional CFD Simulations of A Wind Turbine Blade Section; Validation". Journal of Engineering Science & Technology Review. December 2017. Vol. 11-1. p.138-145. DOI: https://doi.org/10.25103/jestr.111.16
[30] Sahin i, Acir A. "Numerical and experimental investigations of lift and drag performances of NACA 0015 wind turbine airfoil". International Journal of Materials, Mechanics and Manufacturing. February 2015. Vol. 3-1. p.22-25. DOI: https://doi.org/10.7763/IJMMM.2015.V3.159
[31] Zhang P F, Liu A B, Wang J J. "Aerodynamic modification of NACA 0012 airfoil by trailing-edge plasma gurney flap". AIAA Journal. October 2009. Vol. 47-10. p.2467-2474. DOI: https://doi.org/10.2514/1.43379
[32] Ghadimi P, Tanha A, Tavakoli S, et al. "Rans Simulation of the Tip Vortex Flow Generated around a Naca 0015 Hydrofoil and Examination of Its Hydrodynamic Characteristics". Journal of Marine Engineering & Technology. June 2017. Vol. 17-2. p.106-119. DOI: https://doi.org/10.1080/20464177.2017.1330181
[33] Zhang H, Wu Q, Li Y, et al. "Numerical Investigation of the Deformation Characteristics of a Composite Hydrofoil with Different Ply Angles". Ocean Engineering. September 2018. Vol. 163. p.348-357. DOI: https://doi.org/10.1016/j.oceaneng.2018.05.064

APPRECIATION

This study was funded by the Natural Science Foundation of China under Grant No. 51806053 and Anhui Provincial Key Research and Development Program under Grant No. 1804a09020012 and 1804a09020007.

SUPPLEMENTARY MATERIAL

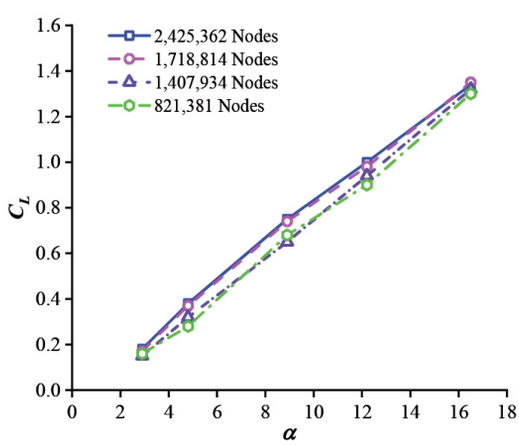

Fig. 3. Grid independence test of NACA0015 hydrofoil at Reynolds number 1E6.